Presented at the 28th European PV Solar Energy Conference and Exhibition, 30 September – 4 October, 2013, Paris, France

A PASSIVATED REAR CONTACT FOR HIGH-EFFICIENCY *n*-TYPE SILICON SOLAR CELLS ENABLING HIGH V_{OC}S AND *FF*>82%

F. Feldmann, M. Bivour. C. Reichel, M. Hermle, S. W. Glunz
Fraunhofer Institute for Solar Energy Systems (ISE)
Heidenhofstrasse 2, D-79110 Freiburg, Germany
Email: frank.feldmann@ise.fraunhofer.de

ABSTRACT: Due to the improvements in material quality and surface passivation, high-efficiency solar cells are often limited by the recombination at the metal semiconductor contacts. As a solution to this problem, Swanson proposed "*to put a heterojunction with a band-gap larger than silicon between the metal and silicon*"[1] also known as passivated contact. In this work, a tunnel oxide passivated contact (*TOPCon*) structure allowing both an excellent surface passivation and an effective carrier transport is presented. High-efficiency *n*-type solar cells featuring this novel passivated rear contact instead of a point contact structure at the rear side yield a maximum efficiency of 23.7 %, a *FF* of 82.2 % and a V_{oc} of 703 mV.

Keywords: Passivation, High-Efficiency, n-type, Silicon Solar Cell

1 INTRODUCTION

In 1985 Yablonovich stated that an ideal solar cell should "be built in the form of a double heterostructure", which would place the absorber between two wide-gap materials of opposite doping [2]. These semi-permeable membranes must ensure that the electrochemical energy (splitting of the quasi-Fermi levels) is completely converted into electrical energy [3]. A famous example is the HIT solar cell [4], achieving very high conversion efficiencies by making use of a heterojunction based on hydrogenated amorphous silicon (a-Si:H), which effectively suppresses recombination at the a-Si:H and crystalline silicon (c-Si) interface as well as at the metal contacts. However, the temperature restrictions of the a-Si:H layers require a dedicated back-end processing (low-temperature deposition of transparent conductive oxide (TCO) and metallization). A temperature-stable approach is based on semi-insulating polysilicon (SIPOS), which was originally used as a passivation layer for silicon devices [5] and thence successfully implemented as an emitter in heterojunction transistors [6]. Its potential for photovoltaics was demonstrated by Yablonovich's SIPOS solar cell, which achieved an impressively high V_{oc} of 720 mV [2]. In addition to SIPOS, the herein proposed passivated contact is closely related to the poly emitter technology, which significantly enhanced current gains of bipolar junction transistors [7]. The successful commercial application of the polysilicon emitter technology in high-speed logic circuits in the 80's urged some researchers to apply these polysilicon contacts to solar cells with the aim to boost V_{oc} [8], [9], [10].

Our approach, which we have called *TOPCon* (Tunnel Oxide Passivated Contact) is based on these prior approaches and consists of an ultra-thin tunnel oxide and a phosphorus-doped silicon layer [11]. It offers a simple processing scheme which is compatible with high-temperature processes such as diffusion.

To obtain highly efficient passivated contacts for solar cells, the following three prerequisites are to be met: (i) excellent interface passivation, (ii) efficiently doped layers to maintain the quasi-Fermi level separation in c-Si (high V_{oc}), and (iii) an efficient majority carrier transport (high *FF*s). To study the performance of our passivated contacts, their interface passivation is tested for by lifetime measurements, and prerequisites (ii) and (iii) are investigated on n-type silicon solar cells with a diffused boron-doped emitter on the front side and the newly developed passivated contacts on the rear side. Furthermore, we examine the cell's light trapping scheme with a focus on an appropriate rear metallization. Finally, the limitations arising from the front grid metallization are discussed and a solution is proposed to reach efficiencies well above 24 %.

2 EXPERIMENTAL DETAILS AND RESULTS

2.1 Interface passivation and its impact on device performance

The interface passivation quality of this passivated contact was determined on symmetrical lifetime samples by the quasi-steady-state photoconductance (QSSPC) technique [12]. Here, the implied open-circuit voltage iV_{oc} at one sun, which is calculated by

$$1)\qquad iV_{oc} = \frac{kT}{q}\ln\left(\frac{\Delta n(\Delta n + N_D)}{n_i^2}\right)$$

is used as a measure for interface passivation. Shiny-etched n-type 1 Ω cm (100)-oriented floating zone (FZ) silicon wafers with a thickness of 200 µm were cleaned according to the RCA cleaning procedure [13]. Then an ultra-thin wet chemical oxide layer was grown with a thickness determined to be about 14 Å by spectroscopic ellipsometry. It should be noted, that 20 Å is the maximum tolerable oxide thickness for the related metal-insulator-semiconductor (MIS) solar cells at which tunneling becomes inefficient and, thus, results in a lowered *FF* [14]. Subsequently, a 20 nm thick phosphorus-doped Si layer was deposited on both sides. Afterwards, the samples' passivation was activated in a tube furnace process with plateau temperatures in the range of 600 °C<T_{anneal}<1000 °C. Fig. 1 plots the iV_{oc} at 1 sun over T_{anneal}. It can be seen that a good passivation can be obtained already after deposition of the Si layer. Depending on the annealing conditions, the good initial passivation can be further boosted to very high implied voltages (iV_{oc} well above 710 mV). To relate our achievements with results from prior art, the corresponding J0,rear values of lifetime samples with iV_{oc} >710 mV were determined using the method proposed by Kane and

Swanson [15]. $J_{0,rear}$ values in the range of 9 to 13 fA/cm² were measured and show that our passivated contacts perform equally well as SIPOS (10 fA/cm²) [2] and as polyemitters with deliberately grown interfacial oxide (20 fA/cm²) [10].

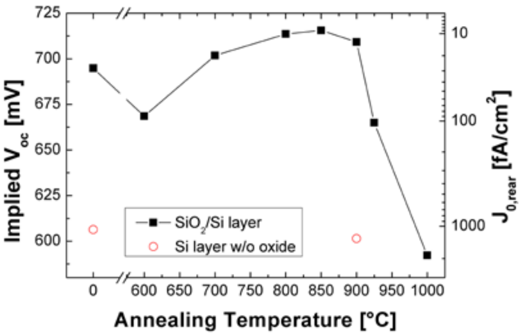

Figure 1: The diagram depicts the implied V_{oc} of *TOPCon*'s interface passivation as a function of the plateau temperature T_{anneal} of the furnace anneal. The samples without tunnel oxide (red circles) clearly underline the importance of the tunnel oxide layer for surface passivation. Additionally, the right y-axis depicts the corresponding $J_{0,rear}$ values calculated according to Eq. 3.

For T_{anneal}>900 °C, a strong decrease in the interface passivation is observed. This can be explained with the local disruption of the SiO2 tunnel junction in oxygen-free ambient according to the reaction SiO_2(s) + Si(s) → 2 SiO(g), where s and g denote the solid and gaseous phase, respectively. This balling-up of oxide was also observed for polyemitter devices with deliberately grown interfacial oxides [16] and inevitably leaves behind large areas of unpassivated silicon in direct contact with the Si layer. Notably, the tunnel oxide is crucial to obtain very high passivation quality, since lifetime samples solely passivated by an as-deposited Si layer or an annealed Si layer (red circles in Fig. 1) yield very low iV_{oc} values. A similar behavior for polyemitter contacts was observed by Kwark et al [10].

Apart from a high V_{oc}, passivated contacts must also provide low interface recombination at MPP conditions to allow for high *FF*s [17]. Provided that the device would only be limited by Auger recombination, the upper limit for the fill factor FF_0 [18, 19] is 89 %. In Fig. 2 an injection-dependent effective minority carrier lifetime-curve $\tau_{eff}(\Delta n)$ is shown and the implied solar cell parameters iV_{oc} and iV_{MPP} are marked, respectively. The implied iV_{MPP} is obtained from the implied J-V curve calculated from the $\tau_{eff}(\Delta n)$ curve and can be understood as a similar measure for device performance as the *PFF* is for SunsVoc measurements [20]. While Auger recombination dominates at open-circuit (OC) conditions, the device does not operate close to the Auger limit at iV_{MPP}. However, a high implied fill factor *iFF* of about 85 % is still obtained. To approach the ideal FF_0 of 89 %, the interface passivation at MPP conditions must be even further enhanced to shift iV_{MPP} into the Auger recombination regime. The reduced passivation quality of the unpassivated lifetime samples (without tunnel oxide) leads thus not only to a lower iV_{oc} but also to a reduced *iFF* of about 83 % (not shown in Figure 2).

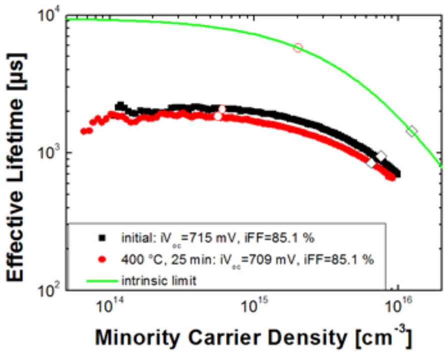

Figure 2: Measured injection dependent effective minority carrier lifetime for a sample symetrically passivated by the *TOPCon* structure after thermal treatment at 800 °C and subsequent hotplate annealing at 400 °C for 25 min, respectively. The figure also depicts the open-circuit (1 sun, open diamonds) and MPP conditions (open circles) as well as the intrinsic limit of the absorber calculated according to [19].

While the passivated contact easily withstands typical diffusion temperatures, its interface passivation after the activation process should be stable at temperatures in the range of 400 °C to provide more opportunities for back-end processing. A typical process such as contact sintering and silicidation was simulated quite realistically by hotplate annealing of the symmetrical lifetime samples at 400 °C. In Fig. 2 it can be observed that the passivation quality and iV_{oc} values above 700 mV can be maintained during the applied annealing conditions. Thus, the passivated contact imposes fewer restrictions on back-end processing compared to classical a-Si:H based passivation schemes.

2.2 Transport characteristics of solar cells with a passivated rear contact

To investigate whether this passivated contact would be an efficient majority carrier contact, it was implemented at the rear side of n-type silicon solar cells with a diffused boron-doped emitter (140 Ω/sq) at the front side (see Fig. 3). The cells (2×2 cm²) were processed on n-type 1 Ωcm FZ silicon wafers. They feature a front surface with random pyramids and a passivated boron-diffused emitter. The 20 µm wide fingers were realized by thermal evaporation of a Ti/Pd/Ag seed layer and subsequent electroplating of Ag. The *TOPCon* structure at the rear surface was deposited and activated following emitter diffusion and drive-in anneal.

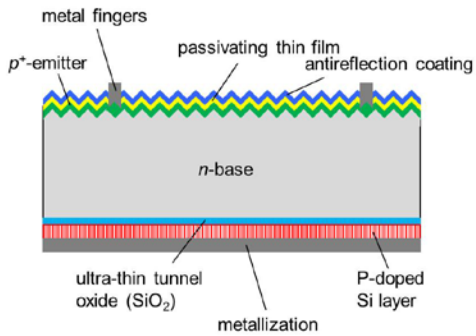

Figure 3: Solar cell with boron-doped emitter at the front and passivated rear contacts.

Table 1 lists the corresponding solar cell results for cells with passivated rear contacts and for those labelled "unpassivated" rear contacts, which do not employ the passivating tunnel oxide.

Table 1: Solar cell parameters of cells with passivated rear contact and unpassivated rear contact (without tunnel oxide).

	V_{oc} [mV]	J_{sc} [mA/cm^2]	*FF* [%]	*PFF* [%]	η [%]
		Passivated rear contact			
Average	690.4	38.4	81.9	84.5	21.7
(7 cells)	±0.9	±0.1	±0.2	±0.0	±0.1[1]
Best	**690.8**	**38.4**	**82.1**	**84.5**	**21.8**[1]
		Unpassivated rear contact			
Average	637.7	37.7	81.2	83.6	19.5
(7 cells)	±0.5	±0.1	±0.1	±0.0	±0.0
Best	**638.3**	**37.8**	**81.1**	**83.6**	**19.6**

[1]Solar cell results are independently confirmed by Fraunhofer ISE Callab.

Most importantly, the tunnel oxide layer needed for passivation does not hinder majority charge carrier transport across its barrier and thus allows for excellent *FF*s of above 82 %. From SunsV_{oc} measurements [21] we obtained a *PFF* of 84.5 %, which is the result of low device recombination at MPP conditions. The small difference between *PFF* and *FF* translates into a very low series resistance of $R_{S,SunsVoc}$=0.41 Ωcm², which is calculated according to

$$2)\quad R_{S,SunsVoc} = (PFF - FF)\frac{V_{oc}J_{sc}}{J_{mpp}^2}. [22]$$

Additionally, the light I-V method [23], which compares the light I-V curve with the J_{sc}-shifted dark I-V curve, was utilized to confirm the result obtained from the SunsV_{oc}-method. Here, $R_{S,light}$=0.37 Ωcm² corroborates above calculation. The individual contributions to R_S can be easily identified by TLM measurements of the specific contact resistances in conjunction with simple spread-sheet calculations according to Goetzberger [24]. Due to a small finger pitch (800 µm) and silver's very low resistivity (ρ_{met}=1.6 µΩcm), the lateral transport in the emitter and series resistance of the fingers make minor contributions ($R_{emitter}$=0.08 Ωcm² and R_{finger}=0.07 Ωcm²). On the other hand, the grid's specific contact resistance ρ_c is determined to be as high as 9 mΩcm², which translates into an upper value for the contact resistance at the diffused emitter of about 0.35 Ωcm². While the passivated contact's specific contact resistance takes a value of about 10 mΩcm², its contribution to R_S can be neglected since the rear is fully metallized. Thus, the relatively small loss in *FF* due to series resistance can be solely attributed to the solar cell's front side.

While solar cells with point contact rear side passivation schemes (e.g. PERL) trade off V_{oc} for *FF* [25], the proposed passivated contact decouples the absorber's passivation from the metallization. Thus, the latter allows for a one-dimensional carrier transport in the base, thereby leading to a *FF* which is more than 1 % absolute higher than the *FF* of a PERL solar cell featuring a similar front side [26]. Furthermore, the cells without oxide layer stress the importance of a low device recombination at MPP conditions. While the *FF* is absolutely 1 % lower compared to the cells with the passivated rear contacts, the series resistance remains the same ($R_{S,SunsVoc}$=0.40 Ωcm²). Thus, the loss in *FF* can be ascribed to a lower *iFF* (as observed in Sec. 1.1) which reduces the *PFF* to 83.6 %.

In addition to the high *FF*, a good V_{oc} as high as 691 mV can be obtained with this solar cell structure. In order to determine the weight of front and rear recombination, the J_0 value is calculated by

$$3)\quad J_0 = J_{0,e} + J_{0,b} = J_{0,e} + J_{0,rear} + qn_i^2\frac{W}{N_D\tau_p},$$

where n_i=8.3x109 cm-3 [27] and τ_p=3.4 ms is the Auger lifetime after [28]. Although this analysis is only valid for low level injection conditions and, thus, prone to error in the case of n-type cells with N_D=5x10^{15} cm^{-3}, it is nevertheless a useful approximation unveiling the limiting factors. While the emitter is well passivated ($J_{oe,pass}$=11 fA/cm²), the unpassivated metal-semiconductor front contacts are the dominant source for recombination ($J_{oe,contact}$=1800 fA/cm²) and constitute an intrinsic loss mechanism of homojunction solar cells. With a metallized area fraction of about 3 %, the total J_{oe} of 64 fA/cm² results in an upper limit (J_{ob}=0) for the cell's V_{oc} of about 700 mV. Taking into account the very low contribution of the rear contact ($J_{0,rear}$=9 fA/cm²) and the base (total J_{0b}=22 fA/cm²) to the cell's recombination current yields a V_{oc} of about 690 mV. Thus, the V_{oc} gap of >20 mV between the solar cells and the lifetime samples can be mainly attributed to the recombination at the unpassivated metal-semiconductor front contacts.

As expected, the V_{oc} of the solar cells with an unpassivated contact (without tunnel oxide layer) is drastically decreased to 638 mV due to a high J_{ob}=593 fA/cm².

2.3 High-efficiency solar cells

To further increase the efficiency, we optimized the solar cell design in terms of light-trapping, device recombination, and series resistance. A simple means to increase the V_{oc} is to reduce the recombination at the metal-semiconductor front contacts by decreasing the metallized area fraction from a A_{metal} of approximately 3 % to a of roughly 1.1 %. Thereby, the J_{oe} is reduced to approximately 30 fA/cm² and, thus, the V_{oc} is expected to be slightly above 700 mV. Furthermore, the grid's specific contact resistance ρ_c could be reduced to less than 1 mΩcm² which gives us the opportunity to decrease A_{metal} without facing R_S induced *FF* losses. The relatively low J_{sc} of 38.4 mA/cm² can be boosted by applying a metallization scheme which ensures that most light is internally reflected and not absorbed by the rear metallization. To this end, the strongly absorbing Ti/Pd/Ag rear contact was replaced by either a stack of lowly-doped 200 nm ITO/1 µm Ag or a 1 µm Ag single layer. While for a planar rear a Ag single layer offers superior rear side reflection as demonstrated by Bivour et al. [29], this is not the case for textured (or rough) rear surfaces [30]. Thus, the Ag needs to buffered from the doped Si layer by a TCO with negligible absorption [31]. Fig. 4 plots both the EQE and reflection over wavelength and it can be clearly seen that both the ITO/Ag stack and the Ag single layer improve the internal reflection significantly. Especially, the reflection of the Ag single layer is just slightly lower than the reflection of our PERL solar cells, which feature a thick dielectric layer with a low index of refraction [26].

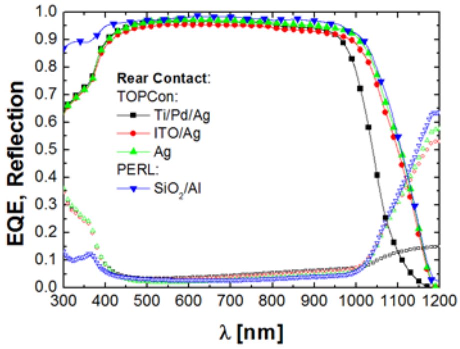

Figure 4: External quantum efficiency (lines and closed symbols) as well as the reflection (open symbols) of solar cells with different rear metallization schemes are plotted over wavelength. Titanium is a very lossy metal and offers very weak reflection above 1000 nm. On the contrary, the stack of ITO/Ag reflects almost as much light as the Ag single layer. The best light management is obtained with our PERL cell (open symbols) [26] featuring a 100 nm SiO_2/Al mirror. Note, the cell's reflection in the wavelenth range below 400 nm and between 600 and 1000 nm is slightly lower due to the use of inverted pyramids and a double antireflection coating.

While both rear metallization schemes improve J_{sc}, only the cells with an Ag single layer achieve *FF*s above 82 % (see Table 2). Contrary to this, the cells with the ITO/Ag stack suffer from a pronounced series resistance, thereby decreasing the *FF* below 75 % (not shown here). Hence, the corresponding results obtained from solar cells with the Ag single layer are given in Table 2. Due to the much higher EQE at long wavelength a very high J_{sc} of more than 41 mA/cm² is achieved. Furthermore, the reduction of A_{metal} of the unpassivated metal-semiconductor front contacts yielded not only the expected V_{oc} gain but also led to a slight *PFF* increase due to a higher FF_0. Therefore, the champion cell has a very high *FF* of 82.6 % and an efficiency of 23.9 %.

Table 2 I-V results of *TOPCon* solar cells featuring a Ag single layer. In addition, the metallized area fraction of the front grid electrodes was varied.

	V_{oc} [mV]	J_{sc} [mA/cm^2]	*FF* [%]	*PFF* [%]	η [%]
		A_{metal}□3.0 %			
Average	692.5	41.1	81.2	84.3	23.1
(21 cells)	±1.4	±0.2	±0.8	±0.4	±0.2
Best	**693.0**	**41.4**	**81.2**	**84.4**	**23.3**
		A_{metal}□1.1 %			
Average	702.5	41.1	82.0	84.7	23.7
(19 cells)	±0.8	±0.1	±0.4	±0.2	±0.1
Best	**703.3**	**41.0**	**82.2**	**84.6**	**23.7**[2]

[2]Best solar cell is independently confirmed by Fraunhofer ISE Callab.

3 SUMMARY

A thermally stable passivated contact for the rear side base contact of n-type silicon solar cells has been presented. It has been shown that our *TOPCon* structure based on a tunnel oxide and phosphorus doped Si layer passivates the surface effectively for both MPP and OC conditions and enables the extraction of V_{oc}s higher than 710 mV. The related J_{0b} value is as low as 22 fA/cm². The solar cells with the *TOPCon* structure have shown excellent performance regarding V_{oc} and *FF*. Contrary to point contact rear side passivation schemes like PERL, its one-dimensional design facilitates processing (no structuring and alignment) and enables high *FF*s above 82 % while maintaining a high V_{oc} above 700 mV. The best cell has an independently confirmed efficiency of 23.7 %. It has also been demonstrated that the efficiency is limited by the recombination at the unpassivated metal-semiconductor front contacts and a viable solution would be a passivated contact for the boron-doped homojunction emitter. Such technology should further increase the efficiency of this solar cell concept well above 24 %.

4 ACKNOWLEDGEMENT

The authors would like to thank A. Leimenstoll, F. Schätzle, S. Seitz, N. Weber, and N. König for sample preparation as well as E. Schäffer for measuring the solar cells. This work was funded by the German Federal Ministry for the Environment, Nature Conservation, and Nuclear Safety under grant No. 0325292"ForTeS".

[1] R. M. Swanson, in Proceedings of the 31st IEEE Photovoltaic Specialists Conference, Orlando, USA, 2005, p. 889.
[2] E. Yablonovitch, T. Gmitter, R. M. Swanson, and Y. H. Kwark, Applied Physics Letters 47 (1985) 1211.
[3] P. Würfel, Physics of Solar Cells - From principles to new concepts, Wiley-Vch Verlag GmbH & Co KgaA, Weinheim, 2005.
[4] T. Kinoshita, D. Fujishima, A. Yano, A. Ogane, S. Tohoda, K. Matsuyama, Y. Nakamura, N. Tokuoka, H. Kanno, H. Sakata, M. Taguchi, and E. Maruyama, in Proceedings of the 26th European Photovoltaic Solar Energy Conference and Exhibition, Hamburg, Germany, 2011, p. 871.
[5] T. Aoki, T. Matsushita, H. Yamoto, H. Hayashi, M. Okayama, and Y. Kawana, Journal of the Electrochemical Society 122 (1975) C82.
[6] T. Matsushita, N. Ohuchi, H. Hayashi, and H. Yamoto, Applied Physics Letters 35 (1979) 549.
[7] I. R. C. Post, P. Ashburn, and G. R. Wolstenholme, IEEE Transactions on Electron Devices 39 (1992) 1717.
[8] N. G. Tarr, Electron Device Letters, IEEE 6 (1985) 655.
[9] F. A. Lindholm, A. Neugroschel, M. Arienzo, and P. A. Iles, Electron Device Letters, IEEE 6 (1985) 363.
[10] Y. H. Kwark and R. M. Swanson, Solid State Electronics 30 (1987) 1121.
[11] F. Feldmann, M. Bivour, C. Reichel, M. Hermle, and S. W. Glunz Solar Energy Materials & Solar Cells (accepted for publication) (2013)
[12] R. A. Sinton, A. Cuevas, and M. Stuckings, in Proceedings of the 25th IEEE Photovoltaic Specialists Conference, IEEE; New York, NY, USA, Washington DC, USA, 1996, p. 457.

[13] W. Kern, Journal of the Electrochemical Society 137 (1990) 1887.
[14] J. Shewchun, R. Singh, and M. A. Green, Journal of Applied Physics 48 (1977) 765.
[15] D. E. Kane and R. M. Swanson, in Proceedings of the 18th IEEE Photovoltaic Specialists Conference, Las Vegas, Nevada, USA, 1985, p. 578.
[16] G. R. Wolstenholme, N. Jorgensen, P. Ashburn, and G. R. Booker, Journal of Applied Physics 61 (1987) 225.
[17] M. Reusch, M. Bivour, M. Hermle, and S. W. Glunz, in SiliconPV, Energy Procedia, Hamelin, Germany, 2013.
[18] M. A. Green, Solar Cells 7 (1981) 337.
[19] A. Richter, S. W. Glunz, F. Werner, J. Schmidt, and A. Cuevas, Physical Review B 86 (2012)
[20] R. A. Sinton and A. Cuevas, in Proceedings of the 16th European Photovoltaic Solar Energy Conference (H. Scheer, B. McNelis, W. Palz, H. A. Ossenbrink, and P. Helm, eds.), James & James, London, UK, 2000, Glasgow, UK, 2000, p. 1152.
[21] R. A. Sinton and A. Cuevas, Applied Physics Letters 69 (1996) 2510.
[22] D. Pysch, A. Mette, and S. W. Glunz, Solar Energy Materials & Solar Cells 91 (2007) 1698.
[23] A. G. Aberle, S. R. Wenham, and M. A. Green, in Proceedings of the 23rd IEEE Photovoltaic Specialists Conference, IEEE; New York, NY, USA, Louisville, Kentucky, USA, 1993, p. 133.
[24] A. Goetzberger, J. Knobloch, and B. Voss, Crystalline silicon solar cells, John Wiley & Sons Ltd, Chichester, UK, 1998.
[25] S. Sterk, J. Knobloch, and W. Wettling, Progress in Photovoltaics: Research and Applications 2 (1994) 19.
[26] J. Benick, B. Hoex, M. C. M. van de Sanden, W. M. M. Kessels, O. Schultz, and S. W. Glunz Applied Physics Letters 92 (2008) 253504/1.
[27] K. Misiakos and D. Tsamakis, Journal of Applied Physics 74 (1993) 3293.
[28] A. Richter, F. Werner, A. Cuevas, J. Schmidt, and S. W. Glunz, Proceedings of the 2nd International Conference on Crystalline Silicon Photovoltaics (Siliconpv 2012) 27 (2012) 88.
[29] M. Bivour, C. Reichel, M. Hermle, and S. W. Glunz, Solar Energy Materials and Solar Cells 106 (2012) 11.
[30] S. K. Kim, H. S. Ee, W. Choi, S. H. Kwon, J. H. Kang, Y. H. Kim, H. Kwon, and H. G. Park, Applied Physics Letters 98 (2011)
[31] Z. C. Holman, M. Filipič, A. Descoeudres, S. De Wolf, F. Smole, M. Topič, and C. Ballif, Journal of Applied Physics 113 (2013) 013107.